

# Ionisation of the atomic gas in redshifted radio sources

S. J. Curran<sup>1\*</sup>, R. W. Hunstead<sup>2</sup>, H. M. Johnston<sup>2</sup>, M. T. Whiting<sup>3</sup>, E. M. Sadler<sup>2,3</sup>,  
J. R. Allison<sup>4</sup> and R. Athreya<sup>5</sup>

<sup>1</sup>*School of Chemical and Physical Sciences, Victoria University of Wellington, PO Box 600, Wellington 6140, New Zealand*

<sup>2</sup>*Sydney Institute for Astronomy, School of Physics, The University of Sydney, NSW 2006, Australia*

<sup>3</sup>*CSIRO Astronomy and Space Science, PO Box 76, Epping NSW 1710, Australia*

<sup>4</sup>*Sub-department of Astrophysics; Department of Physics, University of Oxford, Denys Wilkinson Building, Keble Road, Oxford, OX1 3RH, U.K.*

<sup>5</sup>*Indian Institute of Science Education and Research, 900, NCL Innovation Park, Dr Homi Bhabha Road Pune, Maharashtra 411008, India*

Accepted —. Received —; in original form —

## ABSTRACT

We report the results of a survey for HI 21-cm absorption at  $z \lesssim 0.4$  in a new sample of radio sources with the Giant Metrewave Radio Telescope. Of the 11 sources for which there are good data, we obtain zero detections, where four are expected upon accounting for the ionising photon rates and sensitivity. Adding these to the previously published values, we confirm that the non-detection of 21-cm absorption in active sources at high redshift is due to photo-ionisation of the gas rather than excitation by 21-cm photons (significant at  $6.09\sigma$  and  $2.90\sigma$ , respectively). We also confirm a strong correlation between the absorption strength and the reddening of the source, suggesting that dust plays a significant role in shielding the gas from the ambient ultra-violet field. An anti-correlation between the 21-cm detection rate and the radio turnover frequency is also found, which runs contrary to what is expected on the basis that the higher the turnover frequency, the more compact the source. It is, however, consistent with the hypothesis that the turnover frequency is related to the electron density, supported by a correlation between the turnover frequency and ionising photon rate.

**Key words:** galaxies: active – quasars: absorption lines – radio lines: galaxies – radio continuum: galaxies – galaxies: fundamental parameters – galaxies: ISM

## 1 INTRODUCTION

Cold neutral gas, the reservoir for star formation throughout the Universe, is traced through absorption of the background 21-cm continuum by neutral hydrogen (HI). Beyond the Milky Way, this is either detected in quiescent galaxies, which intervene the sight line to more distant radio sources, or within the host of the continuum source itself. In the former *intervening* systems, absorption via the Lyman- $\alpha$  transition of HI is often also detected (and usually a prerequisite for 21-cm searches), while this is not the case for the latter *associated* systems. This is due to the “proximity effect”, where the absorption by neutral atomic gas (or its tracers, e.g. MgII) becomes sparser as the absorption redshift approaches that of the background source, due to the higher ionising ( $\lambda_{\text{rest}} \lesssim 912$  Å) fluxes (e.g. Weymann et al. 1981; Bajtlik et al. 1988; Wild et al. 2008; Jalan et al. 2018).

A similar effect has been seen for the 21-cm transition, where associated HI 21-cm absorption has never been detected in radio sources above a “critical UV luminosity” of  $L_{\text{UV}} \sim 10^{23}$  W Hz<sup>-1</sup> (Curran et al. 2008), a result which has been confirmed several times since (Curran et al. 2011a, 2013b,c,

2016a, 2017a,b; Allison et al. 2012; Geréb et al. 2015; Aditya et al. 2016; Aditya & Kanekar 2018a; Grasha et al. 2018).<sup>1</sup> This luminosity corresponds to an ionising photon rate of  $Q_{\text{HI}} \equiv \int_{\nu'}^{\infty} (L_{\nu}/h\nu) d\nu \approx 3 \times 10^{56}$  s<sup>-1</sup> (where  $\nu' = 3.29 \times 10^{15}$  Hz), which, from a model of a quasar placed within an exponential gas disk, is just sufficient to ionise all of the neutral gas in a large spiral (Curran & Whiting 2012). This explains the ubiquitous absence of 21-cm absorption in any source with  $Q_{\text{HI}} \gtrsim 3 \times 10^{56}$  s<sup>-1</sup>, at any redshift and independent of source classification. Curran et al. (2008) suggested a selection effect, where the traditional pre-selection of targets of known optical redshifts biases 21-cm surveys towards objects that are the most UV luminous in the source rest-frame. If the gas is completely ionised, even the Square Kilometre Array (SKA) will fail to detect 21-cm absorption in the currently known high redshift radio sources, with future searches being required to dispense with the reliance upon an optical redshift to which to tune the receiver (Curran et al. 2013c; Morganti et al. 2015). Nevertheless, in order to further test this and improve the statistics, we have embarked upon a survey of a new sample of flat

<sup>1</sup> Grasha et al. (2018), which is still in submission, report 0 new detections of HI 21-cm absorption out of 89 new searches over  $0.02 < z < 3.8$  (see Grasha & Darling 2011).

\* Stephen.Curran@vuw.ac.nz

spectrum radio sources over a large redshift space. In Curran et al. (2017a) we reported our  $z \gtrsim 2.6$  survey with the Green Bank Telescope (GBT) and the Giant Metrewave Radio Telescope (GMRT) and here we report our  $z \lesssim 0.4$  GMRT observations.

## 2 SOURCE SELECTION, OBSERVATIONS AND DATA REDUCTION

As in the previous stage of this survey (Curran et al. 2017a), the sources were selected from the *Second Realization of the International Celestial Reference Frame by Very Long Baseline Interferometry* (ICRF2, Ma et al. 2009). This comprises a sample of strong flat spectrum radio sources, of which 1682 now have known redshifts (Titov & Malkin 2009; Titov et al. 2013 and references therein), yielding a frequency to which to tune the receiver in the search for 21-cm absorption. Furthermore, all are VLBI calibrators and so have significant compact flux, thus maximising the chance of a high covering factor and thus optical depth (Curran et al. 2013a, see Sect. 3.1). The goal of the survey was to search and quantify the incidence of associated H I 21-cm absorption over all redshifts and since our previous observations (Curran et al. 2017a) searched 19 sources at  $z \gtrsim 2.6$ , we wished to complement this with lower redshift data. Band-5 of the Upgraded Giant Metrewave Radio Telescope (uGMRT) spans a range of 1000–1450 MHz and, of the ICRF2 sources for which 1420 MHz is redshifted into this range (H I 21-cm at  $z \lesssim 0.42$ ), there are 24 for which the estimated flux density exceeded  $S_{\text{obs}} \approx 0.2$  Jy at the redshifted 21-cm frequency. Of these, there were 23 with sufficient optical/UV photometry to determine the ionising photon rate, of which time was awarded to observe 19 (see Table 1).

In order to strike a balance between sensitivity and sample size, the  $S_{\text{obs}} \geq 0.2$  Jy sources were observed for a total of one hour each, including overheads (calibration and slewing). The observations were taken with the full 30 antenna array on 23 March 2018, in two orthogonal circular polarisations (LL & RR). For bandpass calibration 3C 48, 3C 147 and 3C 298 were used, with the phases being self calibrated. The Band-5 receiver was used with the GSB back-end, over a bandwidth of 16 MHz and 512 channels, giving a spectral resolution of  $\approx 8$  km s<sup>-1</sup> over  $\pm 2000$  km s<sup>-1</sup>, in order to cover any uncertainties in the redshift. The data were calibrated and flagged using the MIRIAD interferometry reduction package. After averaging the two polarisations, a spectrum was extracted from the cube. At these frequencies, radio frequency interference (RFI) was low and a satisfactory image was produced in all but five cases<sup>2</sup> (see Table 1).

## 3 RESULTS

### 3.1 Observational results

In Fig. 1 we show the final spectra, smoothed to a spectral resolution of  $\Delta v = 20$  km s<sup>-1</sup>, and summarise the results in Table 1. The velocity integrated optical depth of the 21-cm absorption,  $\int \tau dv$ , is related to the total neutral hydrogen column density via

$$N_{\text{HI}} = 1.823 \times 10^{18} T_{\text{spin}} \int \tau dv, \quad (1)$$

<sup>2</sup> None of the sources was resolved by the synthesised beam, which ranged from  $3.2'' \times 3.0''$  to  $5.6'' \times 4.5''$ .

where  $T_{\text{spin}}$  is the spin temperature of the gas, which is a measure of the excitation from the lower hyperfine level (Purcell & Field 1956; Field 1959; Bahcall & Ekers 1969). The observed optical depth,  $\tau_{\text{obs}}$ , is the ratio of the line depth,  $\Delta S$ , to the observed background flux,  $S_{\text{obs}}$ , and is related to the intrinsic optical depth via

$$\tau \equiv -\ln \left( 1 - \frac{\tau_{\text{obs}}}{f} \right) \approx \frac{\tau_{\text{obs}}}{f}, \text{ for } \tau_{\text{obs}} \equiv \frac{\Delta S}{S_{\text{obs}}} \lesssim 0.3, \quad (2)$$

where the covering factor,  $f$ , is the fraction of  $S_{\text{obs}}$  intercepted by the absorber. Therefore, in the optically thin regime (where  $\tau_{\text{obs}} \lesssim 0.3$ ), Equ. 1 can be approximated as

$$N_{\text{HI}} \approx 1.823 \times 10^{18} \frac{T_{\text{spin}}}{f} \int \tau_{\text{obs}} dv, \quad (3)$$

which we use to derive the absorption strength sensitivities. Of the 19 targets, the absorption strength could be obtained for 11 which we show in comparison to the previously published values (Fig. 2).<sup>3</sup> Our sensitivities span from  $N_{\text{HI}} = 10^{17.9} - 10^{18.7} T_{\text{spin}}/f$  cm<sup>-2</sup> per 20 km s<sup>-1</sup> channel, which is within the range of the previous detections at  $z \geq 0.1$ .<sup>4</sup>

Note that, although we reach an rms noise level of 18 mJy per 8.41 km s<sup>-1</sup> (giving a  $3\sigma$  a sensitivity to  $N_{\text{HI}} > 2.0 \times 10^{18} T_{\text{spin}}/f$  cm<sup>-2</sup>) in 0003+38A, we do not detect the  $N_{\text{HI}} = 3.5 \times 10^{18} T_{\text{spin}}/f$  cm<sup>-2</sup> absorption of Aditya & Kanekar (2018b) in the cube extracted spectrum. In the  $uv$  data, however, a feature is apparent in the RR polarisation only, with a similar full-width at zero intensity of FWZI  $\approx 50$  km s<sup>-1</sup>, although the feature is shallower (15, cf. 40 mJy) and offset at +1750 km s<sup>-1</sup> (cf. -50 km s<sup>-1</sup>) from  $z = 0.2290$  (i.e. at  $z = 0.2362$ ).

### 3.2 Ionising photon rates

Following the procedure of Curran et al. (2013b), for each source we obtained the photometry from NASA/IPAC Extragalactic Database (NED), the Wide-Field Infrared Survey Explorer (WISE, Wright et al. 2010), *Two Micron All Sky Survey* (2MASS, Skrutskie et al. 2006) and the *Galaxy Evolution Explorer* (GALEX, data release GR6/7)<sup>5</sup> databases. Each flux datum,  $S_\nu$ , was converted to a luminosity, via  $L_\nu = 4\pi D_L^2 S_\nu / (z + 1)$ , where  $D_L$  is the luminosity distance to the source, and corrected for Galactic extinction (Schlegel et al. 1998). A power-law was then fit to the UV rest-frame data, allowing the ionising photon rate,  $Q_{\text{HI}} \equiv \int_\nu^\infty (L_\nu/h\nu) d\nu$ , to be derived.

The derived ionising photon rates shown in comparison to the

<sup>3</sup> These are compiled from de Waard et al. (1985); Mirabel (1989); van Gorkom et al. (1989); Uson et al. (1991); Carilli et al. (1992, 1998, 2007); Moore et al. (1999); Peck et al. (1999, 2000); Röttgering et al. (1999); Morganti et al. (2001); Ishwara-Chandra et al. (2003); Vermeulen et al. (2003); Curran et al. (2006, 2008, 2011a,b, 2013b,c, 2016a, 2017b); Gupta et al. (2006); Orienti et al. (2006); Kanekar et al. (2009); Emonts et al. (2010); Salter et al. (2010); Chandola et al. (2011, 2013); Allison et al. (2012, 2015); Yan et al. (2012, 2016); Geréb et al. (2015); Srianand et al. (2015); Aditya et al. (2016, 2017); Aditya & Kanekar (2018a,b); Curran et al. (2017a); Grasha et al. (2018); Jones et al. (2018); Aditya (2019). Note that, in order to compare our limits with those in the literature, each has been re-sampled to the same spectral resolution (20 km s<sup>-1</sup>, as in Fig. 1). This is used as the FWHM to obtain the integrated optical depth limit, thus giving the  $N_{\text{HI}}f/T_{\text{spin}}$  limit per channel (see Curran 2012).

<sup>4</sup> We restrict our analysis to these redshifts, due to possible weakening of the absorption by coincident 21-cm emission (Curran & Duchesne 2018).

<sup>5</sup> <http://galex.stsci.edu/GR6/#mission>

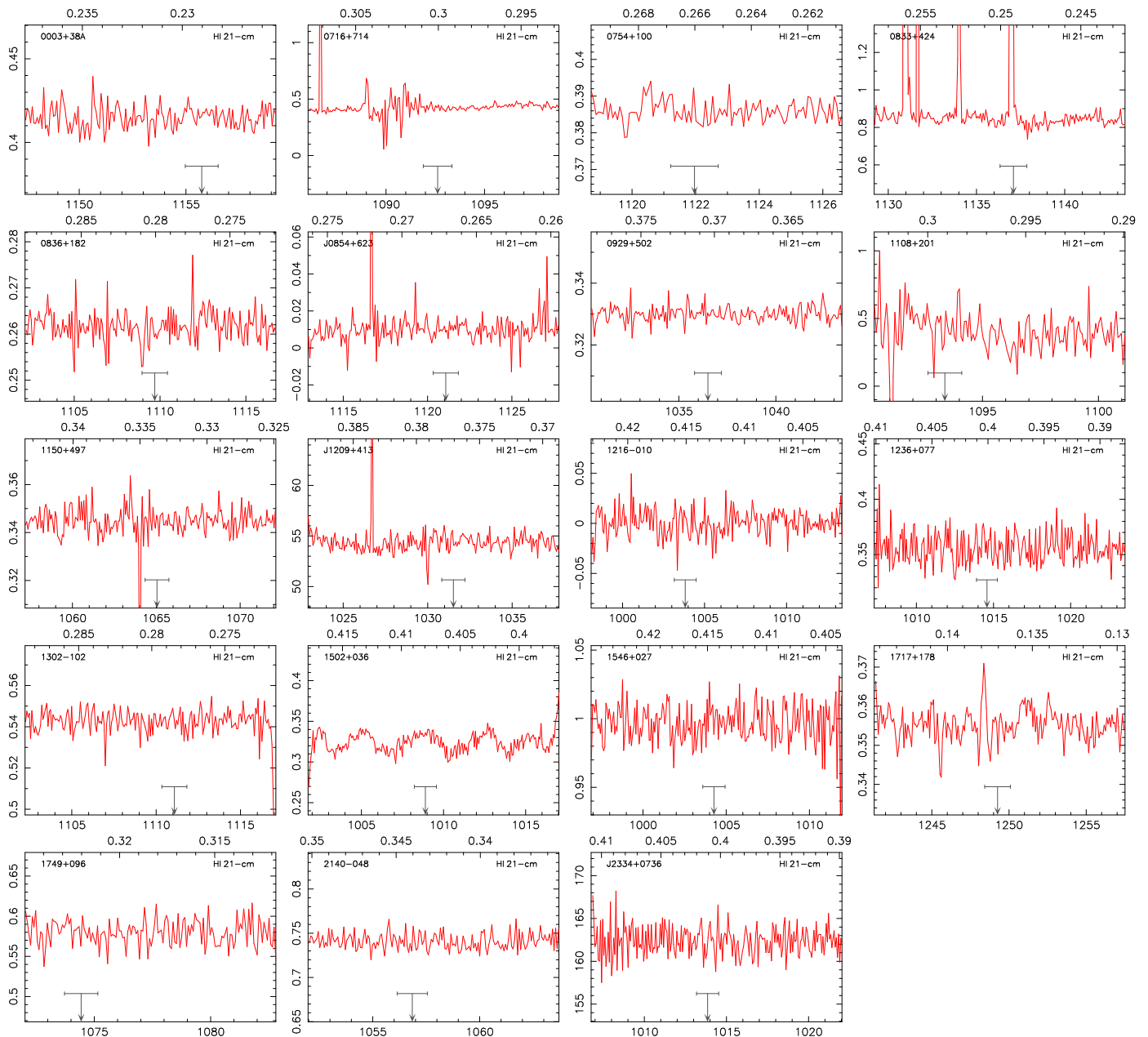


**Figure 1.** The reduced spectra shown at a spectral resolution of  $20 \text{ km s}^{-1}$ . The ordinate gives the flux density [Jy], except for J1209+413 & J2334+0738 (see Table 1), and the abscissa the barycentric frequency [MHz]. The scale along the top shows the redshift of HI 21-cm over the frequency range and the downwards arrow shows the frequency of the absorption expected from the optical redshift, with the horizontal bar showing a span of  $\pm 200 \text{ km s}^{-1}$  for guidance. Note that the features in 1150+497 and J1209+413 are also apparent off source in the image and so are not considered to be real.

previously published searches in Fig. 4.<sup>6</sup> Of the 397  $z \geq 0.1$  sources with sufficient UV photometry, there are 58 detections and 252 non-detections with ionising photon rates up to the highest value where 21-cm absorption has been detected ( $Q_{\text{HI}} = 2.45 \times 10^{56} \text{ s}^{-1}$  in PKS 1200+045, Aditya & Kanekar 2018a).<sup>7</sup> Applying this 18.7% detection rate to the  $Q_{\text{HI}} > 2.45 \times 10^{56} \text{ s}^{-1}$  sources,

<sup>6</sup> The spectral energy distributions (SEDs) of our targets are shown in Fig. 3 of the published version.

<sup>7</sup> Note that Aditya et al. (2017) detect 21-cm absorption at  $z = 1.223$  in TXS 1954+513 for which they claim  $L_{\text{UV}} \approx 4 \times 10^{23} \text{ W Hz}^{-1}$ . This, however, is extrapolated from just two optical (*R*-band and *B*-band) photometry points, which we deem insufficient (see Curran et al. 2013b).

gives a binomial probability of  $1.49 \times 10^{-8}$  of obtaining 0 detections out of 87 searches. This is significant at  $5.66\sigma$ , assuming Gaussian statistics, and supports the finding that the lack of detections at high redshift is due to the optical pre-selection of targets biasing towards sources which are sufficiently UV luminous to ionise all the gas in the host (Curran & Whiting 2012).

The ionising photon rates for the targets, not dominated by RFI, are listed in Table 2. The obtained sensitivities span  $N_{\text{HI}} = 0.6 - 3.0 \times 10^{18} T_{\text{spin}}/f \text{ cm}^{-2}$ . At  $N_{\text{HI}} > 3.0 \times 10^{18} T_{\text{spin}}/f$ , there are 65 detections and 122 non-detections below the critical ionising rate, giving a detection rate of 35%. For the 11 targets with  $Q_{\text{HI}} \lesssim 3 \times 10^{56} \text{ s}^{-1}$ , we therefore expect  $3.9 \pm 2.0$  detections where one is obtained (by Aditya & Kanekar 2018b), and so the detection

**Table 1.** The observational results.  $z$  is the optical redshift of the source,  $\Delta S$  the rms noise reached per 20 km s<sup>-1</sup> channel,  $S_{\text{meas}}$  is the measured flux density,  $\tau_{3\sigma}$  the derived limit to the optical depth, where  $\tau_{3\sigma} = -\ln(1 - 3\Delta S/S_{\text{meas}})$  is quoted for these non-detections. These give the quoted column densities [cm<sup>-2</sup>], where  $T_{\text{spin}}$  is the spin temperature and  $f$  the covering factor, followed by the frequency [MHz] and redshift ranges over which the limit applies (between the RFI spikes to either side of the expected redshift).

Name	$z$	$\Delta S$ [mJy]	$S_{\text{meas}}$ [Jy]	$\tau_{3\sigma}$	$N_{\text{HI}}$ [cm <sup>-2</sup> ]	$\nu$ -range [MHz]	$z$ -range
B2 0003+38A	0.229	7.5	0.419	< 0.054	< $2.0 \times 10^{18} T_{\text{spin}}/f$	1147.51–1159.10	0.22543–0.23781
[HB89] 0716+714	0.300	20.7	0.434		RFI DOMINANT	1086.83–1098.54	0.29299–0.30693
[HB89] 0754+100	0.266	2.94	0.386	< 0.023	< $8.3 \times 10^{17} T_{\text{spin}}/f$	1118.81–1126.47	0.26094–0.26957
FBQS J083353.8+422401	0.249153	—	—		RFI DOMINANT	1137.53–1143.13	0.24256–0.24868
[HB89] 0836+182	0.280	3.13	0.262	< 0.036	< $1.3 \times 10^{18} T_{\text{spin}}/f$	1102.33–1116.50	0.27219–0.28855
WISE J085450.56+621850.1	0.267	—	—		RFI DOMINANT	1113.21–1127.59	0.25968–0.27596
WISE J092915.43+501336.0	0.370387	2.47	0.330	< 0.022	< $8.2 \times 10^{17} T_{\text{spin}}/f$	1030.78–1043.15	0.36166–0.37799
PKS 1108+201	0.2991	—	—		RFI DOMINANT	1090.47–1100.93	0.29019–0.30256
SBS 1150+497	0.33366	4.91	0.345	< 0.043	< $1.6 \times 10^{18} T_{\text{spin}}/f$	1064.50–1071.88	0.32516–0.33434
FBQS J120922.7+411941	0.377	—	—		NO FLUX CALIBRATION	1023.36–1037.52	0.36904–0.38798
[HB89] 1216–010	0.415	13.4	—		INSUFFICIENT FLUX	998.13–1013.15	0.40197–0.42307
[HB89] 1236+077	0.400	13.3	0.356	< 0.11	< $4.1 \times 10^{18} T_{\text{spin}}/f$	1007.62–1023.33	0.38802–0.40967
PG 1302–102	0.2784	8.28	0.543	< 0.046	< $1.7 \times 10^{18} T_{\text{spin}}/f$	1102.38–1116.52	0.27217–0.28849
[HB89] 1502+036	0.40788	—	0.324		BANDPASS RIPPLE DOMINANT	1002.11–1016.80	0.39694–0.41742
[HB89] 1546+027	0.41438	13.2	0.997	< 0.040	< $1.4 \times 10^{18} T_{\text{spin}}/f$	997.11–1011.65	0.40405–0.42452
[HB89] 1717+178	0.137	3.63	0.355	< 0.031	< $1.1 \times 10^{18} T_{\text{spin}}/f$	1246.80–1258.66	0.12851–0.13924
[HB89] 1749+096	0.322	15.7	0.580	< 0.081	< $3.0 \times 10^{18} T_{\text{spin}}/f$	1241.37–1257.21	0.12981–0.14422
[HB89] 2140–048	0.344	9.12	0.741	< 0.037	< $1.4 \times 10^{18} T_{\text{spin}}/f$	1052.13–1063.65	0.33541–0.35003
WISE J233412.82+073627.6	0.401	—	—		NO FLUX CALIBRATION	1006.88–1021.98	0.38985–0.41070

Notes: 0003+38A detected at  $N_{\text{HI}} = 3.5 \times 10^{18} (T_{\text{spin}}/f)$  cm<sup>-2</sup> by Aditya & Kanekar (2018b), 0754+100 observed to a sensitivity of  $< 7.3 \times 10^{17} (T_{\text{spin}}/f)$  cm<sup>-2</sup> per 30 km s<sup>-1</sup> channel by Grasha et al. (2018), 1108+201 to  $< 8.1 \times 10^{18} (T_{\text{spin}}/f)$  cm<sup>-2</sup> per 17.8 km s<sup>-1</sup> channel by Aditya & Kanekar (2018a). Flux calibration was not possible for 1206+416 nor J2334+0736, with the task `gpboot` over-scaling the fluxes.

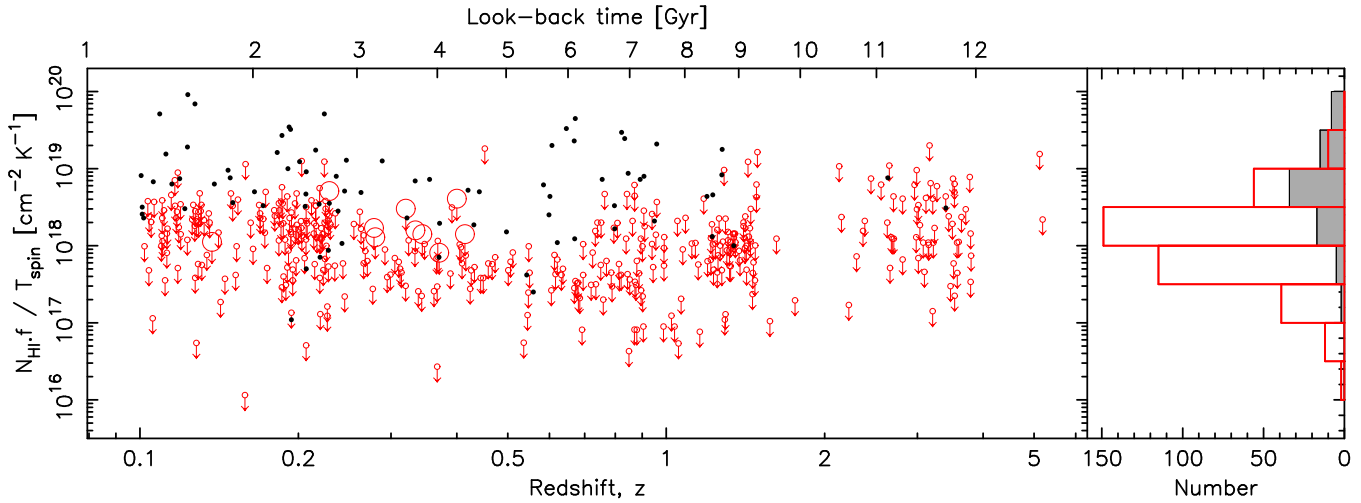


**Figure 2.** The absorption strength [ $1.823 \times 10^{18} (T_{\text{spin}}/f) \int \tau dv$ ] versus redshift for the  $z \geq 0.1$  associated HI 21-cm absorption searches. The filled circles/histogram represent the detections and the unfilled circles/histogram the  $3\sigma$  upper limits to the non-detections, with the large circles designating the new targets (Table 1).

rate is not especially anomalous. This is confirmed by applying the global 18.7% probability of detection below the critical luminosity, which gives a binomial probability of 0.3621 of obtaining one or fewer detections out of 11 searches (significant at just  $0.91\sigma$ ).

Given that the sample is larger with more comprehensive photometry<sup>8</sup>, we now we examine other selection factors, over and above the ionising photon rate, which could affect the 21-cm ab-

sorption detection rate (e.g. the degree of dust reddening and the coverage of the background flux, Curran et al. 2017b).

## 4 DISCUSSION

### 4.1 Photo-ionisation versus excitation by 21-cm photons

Firstly, we examine the suggestion of Aditya et al. (2016); Aditya & Kanekar (2018a,b) that gas excitation by the incident radio continuum may be responsible for the paucity of 21-cm detections at high redshift. As mentioned in Sect. 3.1, the spin temper-

<sup>8</sup> Giving 397 compared to 211 sources previously (Curran et al. 2017a).

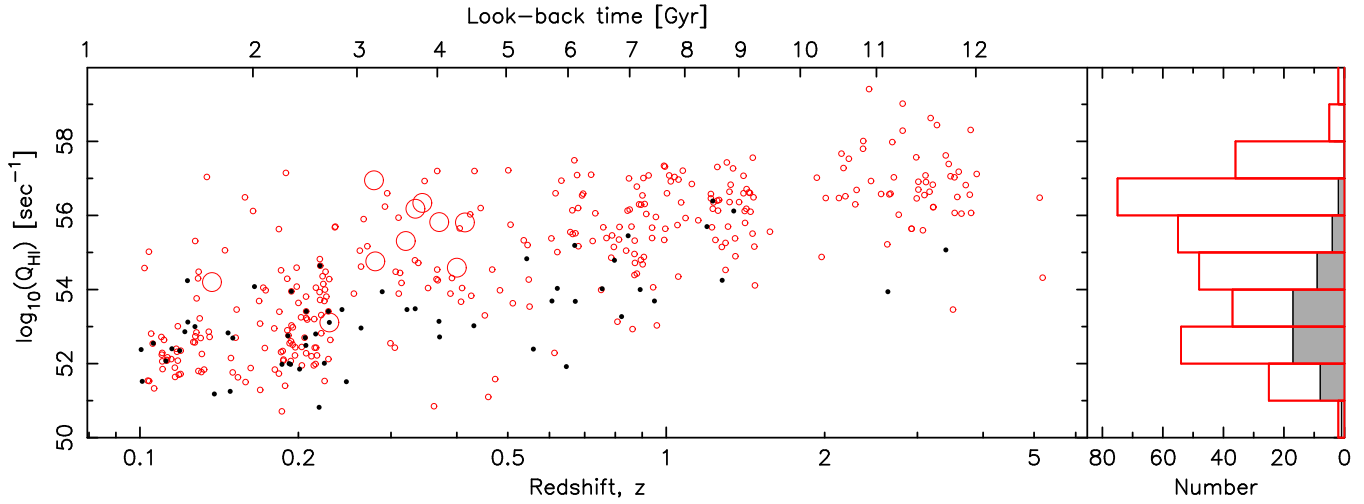


**Figure 4.** The ionising ( $\lambda \leq 912 \text{ \AA}$ ) photon rate versus redshift for the H I 21-cm absorption searches. The symbols and histogram are as per Fig. 2.

**Table 2.** The ionising photon rates for the targets for which we could obtain limits to the 21-cm absorption strength (Table 1).

Source	$z$	$N_{\text{HI}} [\text{cm}^{-2}]$	$Q_{\text{HI}} [\text{s}^{-1}]$
0003+38A	0.229	$3.5 \times 10^{18} T_{\text{spin}}/f$	$1.3 \times 10^{53}$
0754+100	0.266	$< 5.9 \times 10^{17} T_{\text{spin}}/f$	$7.9 \times 10^{55}$
0836+182	0.280	$< 1.3 \times 10^{18} T_{\text{spin}}/f$	$5.8 \times 10^{54}$
J0929+5013	0.370387	$< 8.2 \times 10^{17} T_{\text{spin}}/f$	$6.6 \times 10^{55}$
1108+201	0.2991	$< 4.2 \times 10^{17} T_{\text{spin}}/f$	$3.6 \times 10^{52}$
1150+497	0.33366	$< 1.6 \times 10^{18} T_{\text{spin}}/f$	$1.5 \times 10^{56}$
1236+077	0.400	$< 4.1 \times 10^{18} T_{\text{spin}}/f$	$3.9 \times 10^{54}$
1302-102	0.2784	$< 1.7 \times 10^{18} T_{\text{spin}}/f$	$8.9 \times 10^{56}$
1546+027	0.41438	$< 1.4 \times 10^{18} T_{\text{spin}}/f$	$6.5 \times 10^{55}$
1717+178	0.137	$< 1.1 \times 10^{18} T_{\text{spin}}/f$	$1.6 \times 10^{54}$
1749+096	0.322	$< 3.0 \times 10^{18} T_{\text{spin}}/f$	$2.0 \times 10^{55}$
2140-048	0.344	$< 1.4 \times 10^{18} T_{\text{spin}}/f$	$2.2 \times 10^{56}$

Notes:  $N_{\text{HI}} = 3.5 \times 10^{18} (T_{\text{spin}}/f) \text{ cm}^{-2}$  in 0003+38A from Aditya & Kanekar (2018b),  $< 5.9 \times 10^{17} (T_{\text{spin}}/f) \text{ cm}^{-2}$  in 0754+100 from Grasha et al. (2018) and  $< 4.2 \times 10^{17} (T_{\text{spin}}/f) \text{ cm}^{-2}$  in 1108+201 from Aditya & Kanekar (2018a), upon re-sampling to a spectra resolution of  $20 \text{ km s}^{-1}$ .

ature of the gas can be raised by excitation to the upper hyperfine level by 21-cm photons and the Malmquist bias would cause the high redshift sources to be the most luminous. Due to the detection of 21-cm absorption over all of the same radio luminosities as the non-detections, this was deemed an unlikely cause by Curran et al. (2008), with Curran & Whiting (2010) using the  $T$ -statistic to show that the UV was dominant over the radio luminosity. Since the sample has increased significantly, however, we revisit this. The  $T$ -statistic is given by

$$T = \frac{\hat{p}_1 - \hat{p}_2}{\sqrt{\hat{p}(1 - \hat{p})(N_1^{-1} + N_2^{-1})}},$$

where  $\hat{p}_1 = X_1/N_1$  and  $\hat{p}_2 = X_2/N_2$  are the two measured proportions (i.e. the detection rate below and above the cut) and  $\hat{p} = (X_1 + X_2)/(N_1 + N_2)$  is the total proportion. This has the standard normal distribution under the null hypothesis that the proportions ( $\hat{p}_1$  and  $\hat{p}_2$ ) are the same, which we reject for  $Q_{\text{HI}} \gtrsim 10^{53} \text{ s}^{-1}$ , where the difference between the two proportions is significant at  $> 3\sigma$  (Fig. 5).

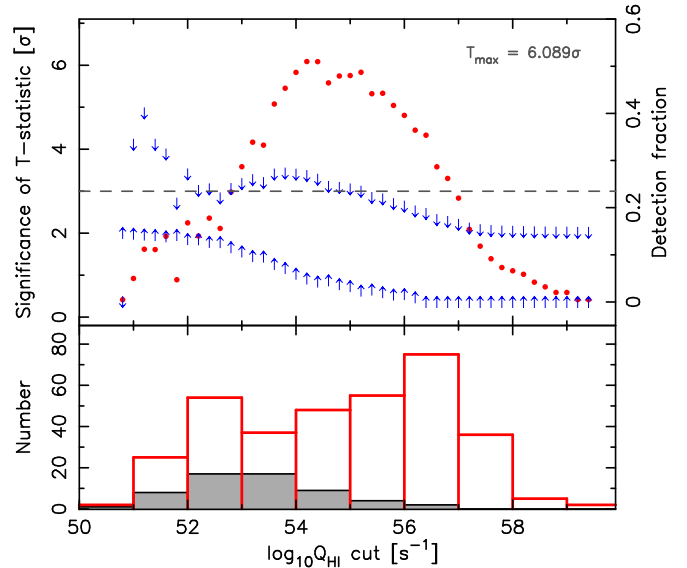


**Figure 5.** The  $T$ -statistic of the difference in the proportions,  $\hat{p}_1$  and  $\hat{p}_2$ , for the detection of H I 21-cm absorption at various cuts of the ionising photon rate. The downward/upwards arrows show the detection fraction (right hand scale) below/above the cut ( $\hat{p}_1$  and  $\hat{p}_2$ , respectively). The significance is seen to drop to  $< 3\sigma$  at  $Q_{\text{HI}} \gtrsim 10^{57} \text{ s}^{-1}$ , due to the lack of detections — shown in the bottom panel, where the filled histogram shows the number of detections and the unfilled the number of non-detections.

In Fig. 6 we show the  $T$ -statistic for the rest-frame 1420 MHz continuum luminosity, obtained from the second order polynomial fit to the radio SEDs. This peaks at  $< 3\sigma$ , indicating that excitation by the continuum radio luminosity has less of an effect on the detection of 21-cm absorption. The increase at  $L_{21\text{-cm}} \gtrsim 10^{26} \text{ W Hz}^{-1}$  is most likely due to the correlation between the radio and UV luminosities, which are both degenerate with redshift (Curran & Whiting 2010).

Examining this further, by including the limits to the absorption strength via the *Astronomy SURVival Analysis* (ASURV) package (Isobe et al. 1986), a generalised non-parametric Kendall-tau test gives a probability of  $P(\tau) = 1.30 \times 10^{-8}$  of the  $N_{\text{HI}}f/T_{\text{spin}} - Q_{\text{HI}}$  anti-correlation occurring by chance (Fig. 7), which is significant at  $S(\tau) = 5.69\sigma$ . For the continuum radio

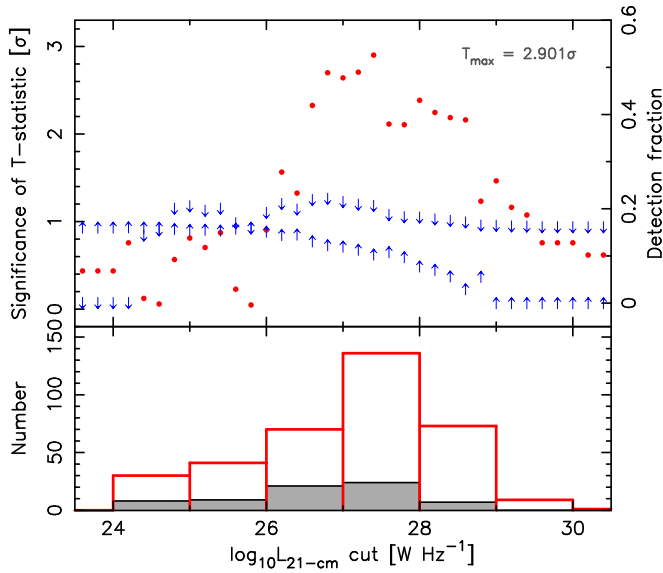


**Figure 6.** As Fig. 5, but for the 21-cm continuum luminosity.

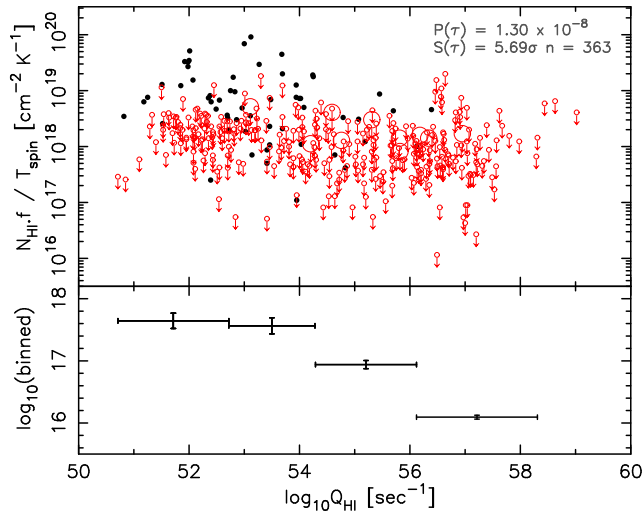


**Figure 7.** The absorption strength versus the ionising photon rate. In the bottom panel, the data are shown in equally sized bins, where the horizontal bars show the range of points in the bin and the vertical error bars the  $1\sigma$  uncertainty in the mean value. The limits are incorporated, via the Kaplan–Meier estimator, which gives a maximum-likelihood estimate based upon the parent population (Feigelson & Nelson 1985).

luminosity, the correlation remains weak (Fig. 8), thus suggesting that photo-ionisation of the neutral gas is the primary reason for the non-detection of 21-cm absorption in the high redshift sources.

## 4.2 Other factors

### 4.2.1 Source reddening

Another factor that is shown to have an effect on the HI 21-cm detection rate is the redness of the source (Webster et al. 1995; Carilli et al. 1998), with Curran et al. (2006, 2017b); Curran & Whiting (2010) finding a correlation between visible (or blue)–near-infrared colour and the absorption strength. Although the visible magnitudes will be degenerate with the ionising photon rate, this may provide evidence of dust shielding the neutral

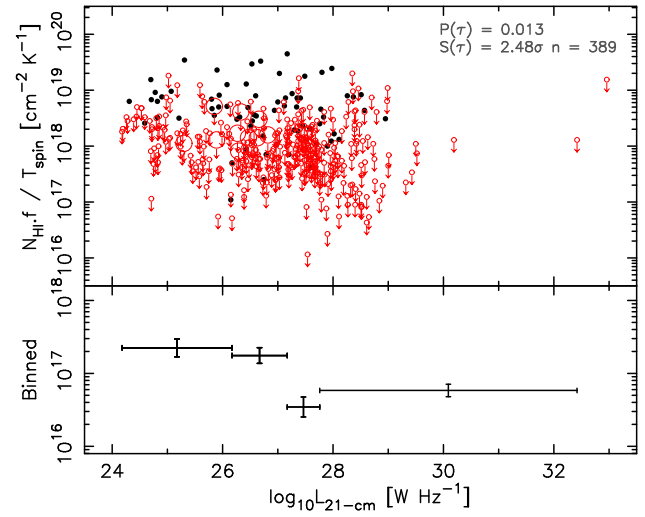


**Figure 8.** The absorption strength versus the 21-cm continuum luminosity.

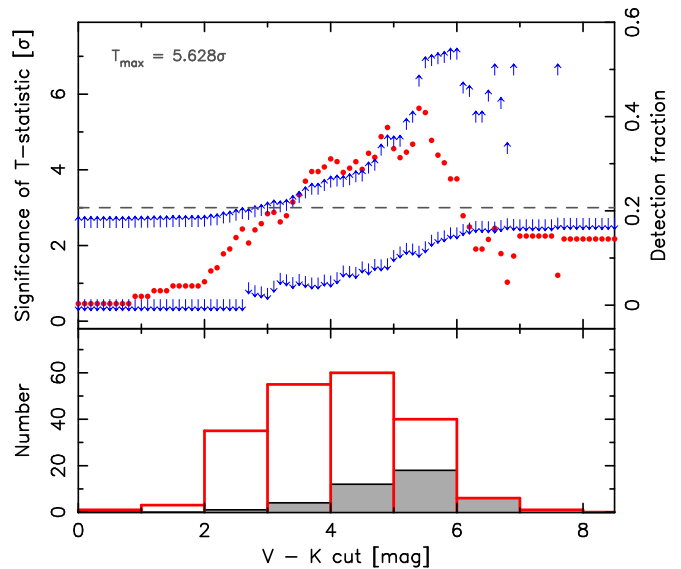


**Figure 9.** As Fig. 5, but for the visible–near-infrared colour.

gas from ambient UV radiation. This effect has also been observed for the molecular absorption strength in intervening absorption systems (Curran et al. 2011), where the absorbing gas is remote from the ionising UV continuum, suggesting that the reddening is indeed at least partially due to dust. This, however, has been recently disputed by Aditya & Kanekar (2018b), who found no correlation between the absorption strength and degree of reddening (through the red–near-infrared colour). Obtaining the visible and near-infrared magnitudes from the photometry fits of the entire sample (Sect. 3.2), in Fig. 9 we show the  $T$ -statistic for the visible–near-infrared colour, from which we see that the degree of reddening has a significant effect on the detection rate at  $V - K \gtrsim 3$ . Furthermore, Fig. 10 demonstrates a strong correlation between the absorption strength and the degree of reddening (and also suggests that our targets may not be sufficiently reddened). This is inconsistent with the finding of Aditya & Kanekar (2018b), who use  $R - K$  – the  $R$ -magnitude will not be as susceptible to dust attenuation as the  $V$ -magnitude. Additionally, they use a smaller (58 cf. 230

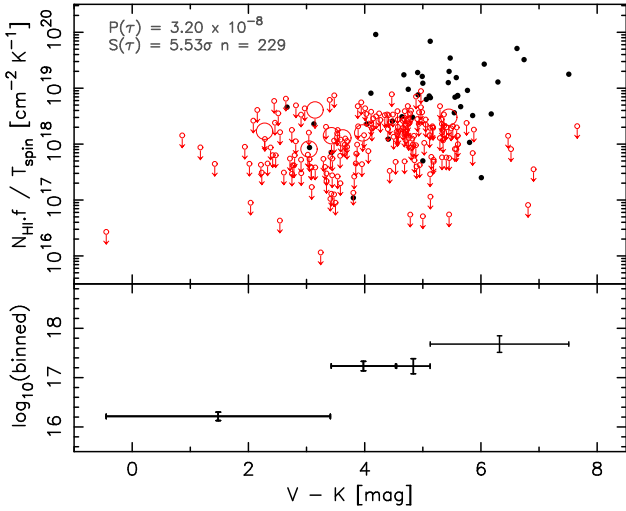


**Figure 10.** The absorption strength versus the visible–near-infrared colour.

sources, for which we could obtain the magnitudes) and more biased (containing  $\alpha_{21\text{-cm}} > -0.5$  sources only) sample.

#### 4.2.2 Spectral index

In addition to excitation of the gas raising the spin temperature, the coverage of the continuum flux can affect the detection of 21-cm absorption: Low coverage ( $f < 1$ ) will reduce the observed optical depth (Equ. 2), as has been observed in the case of intervening absorption (Curran et al. 2005). For associated absorption, the observed optical depth is known to be anti-correlated with the extent of the radio emission, consistent with  $f \propto \tau_{\text{obs}}$  (Curran et al. 2013a).

Generally, the radio emission extents are unknown and the extent of the absorbing medium would also be required to determine the covering factor. One proxy for the covering factor, via the radio source size, is the spectral index. Here, extended radio sources beaming along our sight-line are expected to have flatter radio SEDs than those in which the lobes are projected in the plane of the sky (Fanti et al. 1990). Indeed, Curran et al. (2013b) attributed their non-detections in eight  $L_{\text{UV}} \lesssim 10^{23} \text{ W Hz}^{-1}$  sources to the selection of ultra-steep spectrum ( $\alpha_{21\text{-cm}} \lesssim -1$ ) sources at  $z \gtrsim 3$  (de Breuck et al. 2002). Therefore, any correlation between the spectral index and absorption strength would suggest a strong relationship between the spectral slope and the extent of the radio emission. From the  $T$ -statistic (Fig. 11), we do see that the detections may favour flat spectrum ( $\alpha_{21\text{-cm}} \approx 0$ ) sources, although this is not significant and so could be the result of small numbers at  $|\alpha_{21\text{-cm}}| \gtrsim 1$ .

#### 4.2.3 Turnover frequency

Another tracer of radio source size is the presence of a turnover in the SED, due to free–free absorption/synchrotron self-absorption at low frequencies causing a turnover at  $\nu_{\text{TO}} \sim \text{GHz}$ . In such gigahertz peaked sources (GPS), the turnover frequency is anti-correlated with the source size (e.g. O’Dea 1998; Fanti 2000; Orienti et al. 2006) and a possible correlation between the detection of 21-cm absorption and the turnover frequency was suggested in near-by galaxies, where  $\langle \nu_{\text{TO}} \rangle = 10^{8.66 \pm 0.32} \text{ Hz}$  for the detec-

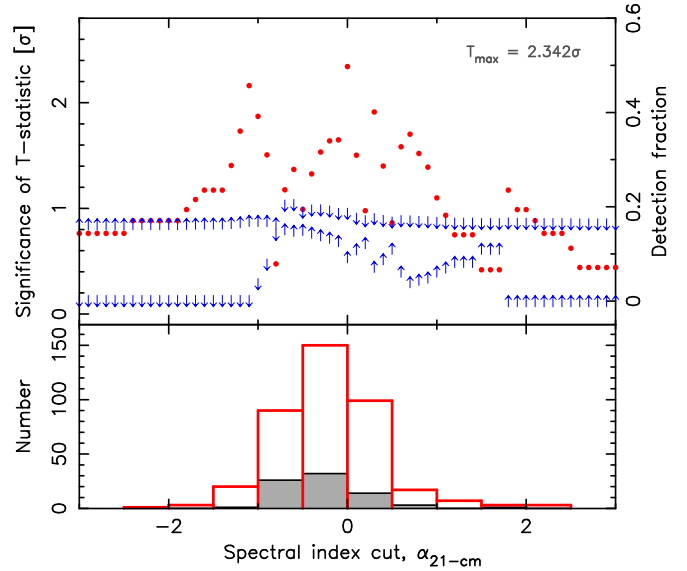


**Figure 11.** As Fig. 5, but for the rest-frame 1420 MHz spectral index (see Sect 4.1).

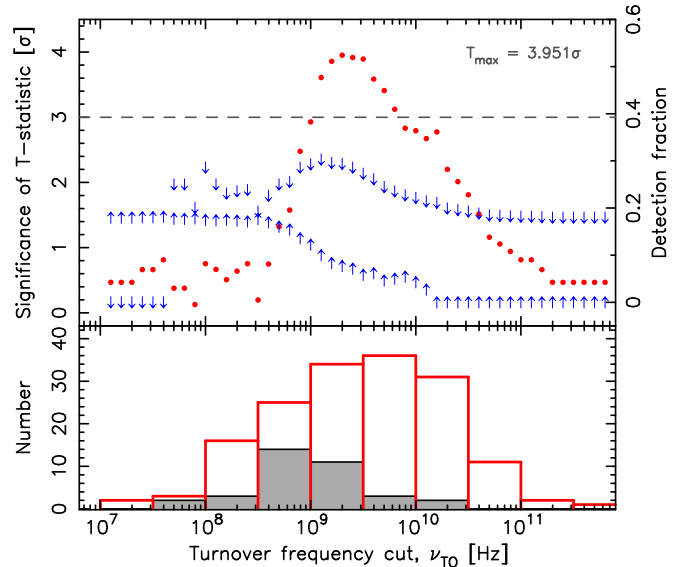


**Figure 12.** As Fig. 5, but for the radio-band turnover frequency.

tions, compared to  $\langle \nu_{\text{TO}} \rangle = 10^{8.00 \pm 0.21} \text{ Hz}$  for the non-detections (Curran et al. 2016b)

For the whole sample, we obtain the rest-frame (intrinsic) turnover frequency from the second order polynomial fit to the radio SEDs (see Curran et al. 2013b), which shows a significant ( $> 3\sigma$ ) effect for  $\nu_{\text{TO}} \gtrsim 1 \text{ GHz}$  (Fig. 12). However, this is due to a lower 21-cm detection rate at higher values of  $\nu_{\text{TO}}$ , which would suggest that the detection rate decreases with the background continuum size, contrary to what we expect from  $f \propto \tau_{\text{obs}}$ . de Vries et al. (1997) showed that the turnover frequency increases with redshift, which they attributed to the higher radio luminosities increasing the electron density. Investigating this, we find only a weak  $\nu_{\text{TO}} - z$  correlation (Fig. 13), which may be driven by the ionising photon rate (Fig. 14), rather than the radio power (Fig. 15). This is consistent with photo-ionisation of the gas increasing the

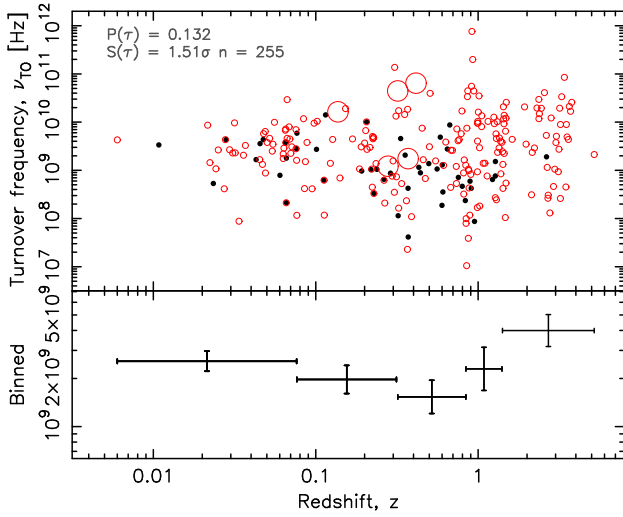


**Figure 13.** The rest-frame turnover frequency versus the redshift for all of the published HI 21-cm absorption searches which exhibit a turnover.

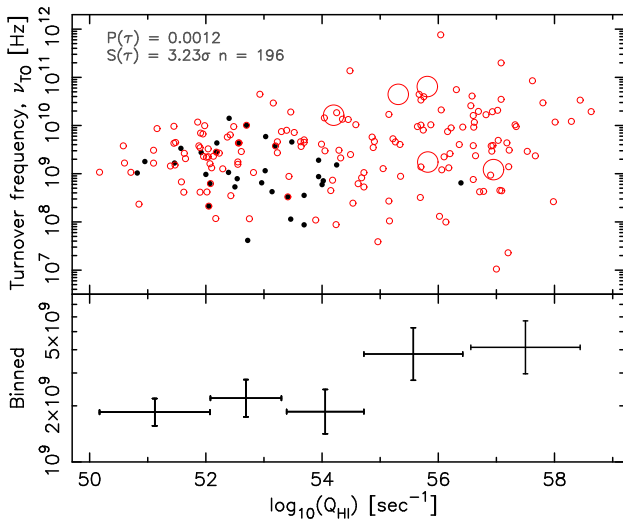


**Figure 14.** As Fig. 13, but for the ionising photon rate.

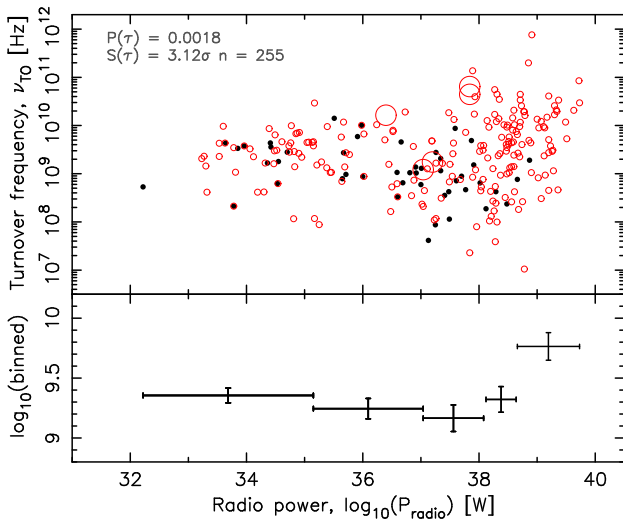


**Figure 15.** As Fig. 13, but for the radio power.

electron density to such an extent that it negates any detection benefit of the smaller source sizes.

## 5 CONCLUSIONS

As part of our ongoing survey to determine the incidence of associated HI 21-cm absorption with redshift, we report on the now complete low redshift phase of this. We have observed 19 compact radio sources at  $z \lesssim 0.4$ , for which we obtain useful spectra for 11. Three of the sources have been previously searched, with one being detected (Aditya & Kanekar 2018a,b; Grasha et al. 2018). Combining these with our useful spectra, gives 11 sources which have ionising photon rates below the critical ionising photon rate, from which we expect four detections, based upon the general detection rate over the sensitivities reached. Given that the statistics have significantly increased, due to a larger sample and more complete photometry, we revisit the main observational factors believed to affect the detection of HI 21-cm absorption:

(i) We confirm that the photo-ionisation of the neutral gas by high ionising ( $\lambda \lesssim 912 \text{ \AA}$ ) photon rates is most likely responsible for the paucity of 21-cm absorption at high redshift. The binomial probability of the exclusive non detections found at ionising photon rates of  $Q_{\text{HI}} \gtrsim 3 \times 10^{56} \text{ s}^{-1}$  is significant at  $5.66\sigma$ , consistent with hypothesis that all of the neutral gas in the host is ionised above these rates (Curran & Whiting 2012).

(ii) The difference between the detection and non-detection fractions reaches a significance of  $6.09\sigma$  for  $Q_{\text{HI}}$ , whereas this peaks at  $2.90\sigma$  for the radio luminosity. This confirms the finding of Curran et al. (2008); Curran & Whiting (2012) that the non-detection of neutral atomic gas at high redshift is dominated by photo-ionisation of the gas, rather than excitation to the upper hyper-fine level by 1420 MHz photons (Aditya et al. 2016; Aditya & Kanekar 2018a,b).

(iii) We confirm that the reddening of the source is correlated with the strength of the 21-cm absorption (Curran et al. 2006, 2017b; Curran & Whiting 2010), with a  $5.53\sigma$  correlation between visible–near-infrared colour and absorption strength. A low degree of reddening will, of course, be degenerate with the faint observed  $V$  magnitudes in the UV luminous sources, although the fact that this is also seen for intervening absorbers (Curran et al. 2011) suggests that at least some of the reddening is due to the presence of dust.

(iv) That the detection rate shows no strong dependence on the radio-band spectral index, which is believed to trace the projected extent of the background source size and thus the coverage of the flux by the absorber. However, the majority of the sources are flat spectrum with  $|\alpha_{21-\text{cm}}| \lesssim 0.5$ .

(v) Since the source size is anti-correlated with radio turnover frequency for gigahertz peaked sources, we also expect a correlation with the detection rate. We do find a strong relationship, although this is in the opposite sense to that expected with the detection rate decreasing with  $\nu_{\text{TO}}$ , where the source sizes are believed to be smaller (O’Dea 1998; Fanti 2000; Orienti et al. 2006). This is, however, consistent with the turnover frequency increasing with redshift, although it is possible that the main driver is the higher ionising photon rate rather than higher radio power (de Vries et al. 1997). It does, nevertheless, support their argument that higher turnover frequencies are a tracer of higher electron densities in gigahertz peaked sources.

Thus, we conclude that photo-ionisation of the gas is the main fac-



tor in rendering detections of H I 21-cm absorption rare at redshifts of  $z \gtrsim 1$ : A high redshift source sufficiently bright to provide a spectrum in the optical band is extremely UV luminous in the source rest-frame, thus introducing a selection effect where the optical pre-selection of targets biases against the sources most likely to contain large quantities of cool neutral gas. Again, this appears to be independent of the radio properties, implying an ubiquitous effect, and reinforces our conclusion that the pre-selection of targets based upon the optical spectra must be foregone in favour of wide-band radio observations.

## ACKNOWLEDGEMENTS

We wish to thank the anonymous referee for their prompt and helpful comments. We also thank the staff of the GMRT who have made these observations possible. GMRT is run by the National Centre for Radio Astrophysics of the Tata Institute of Fundamental Research. The National Radio Astronomy Observatory is a facility of the National Science Foundation operated under cooperative agreement by Associated Universities, Inc This research has made use of the NASA/IPAC Extragalactic Database (NED) which is operated by the Jet Propulsion Laboratory, California Institute of Technology, under contract with the National Aeronautics and Space Administration. This research has also made use of NASA's Astrophysics Data System Bibliographic Services and ASURV Rev 1.2 (Lavalley et al. 1992), which implements the methods presented in Isobe et al. (1986).

## REFERENCES

- Aditya J. N. H. S., 2019, *MNRAS*, 482, 5597  
 Aditya J. N. H. S., Kanekar N., 2018a, *MNRAS*, 473, 59  
 Aditya J. N. H. S., Kanekar N., 2018b, *MNRAS*, 481, 1578  
 Aditya J. N. H. S., Kanekar N., Kurapati S., 2016, *MNRAS*, 455, 4000  
 Aditya J. N. H. S., Kanekar N., Prochaska J. X., Day B., Lynam P., Cruz J., 2017, *MNRAS*, 465, 5011  
 Allison J. R. et al., 2012, *MNRAS*, 423, 2601  
 Allison J. R. et al., 2015, *MNRAS*, 453, 1249  
 Bahcall J. N., Ekers R. D., 1969, *ApJ*, 157, 1055  
 Bajtlik S., Duncan R. C., Ostriker J. P., 1988, *ApJ*, 327, 570  
 Carilli C. L., Menten K. M., Reid M. J., Rupen M. P., Yun M. S., 1998, *ApJ*, 494, 175  
 Carilli C. L., Perlman E. S., Stocke J. T., 1992, *ApJ*, 400, L13  
 Carilli C. L., Wang R., van Hoven M. B., Dwarakanath K., Chengalur J. N., Wyithe S., 2007, *AJ*, 133, 2841  
 Chandola Y., Gupta N., Saikia D. J., 2013, *MNRAS*, 429, 2380  
 Chandola Y., Sirothia S. K., Saikia D. J., 2011, *MNRAS*, 418, 1787  
 Curran S. J., 2012, *ApJ*, 748, L18  
 Curran S. J., Allison J. R., Glowacki M., Whiting M. T., Sadler E. M., 2013a, *MNRAS*, 431, 3408  
 Curran S. J., Allison J. R., Whiting M. T., Sadler E. M., Combes F., Pracy M. B., Bignell C., Athreya R., 2016a, *MNRAS*, 457, 3666  
 Curran S. J., Duchesne S. W., 2018, *MNRAS*, 476, 3580  
 Curran S. J., Hunstead R. W., Johnston H. M., Whiting M. T., Sadler E. M., Allison J. R., Bignell C., 2017a, *MNRAS*, 470, 4600  
 Curran S. J., Murphy M. T., Pihlström Y. M., Webb J. K., Purcell C. R., 2005, *MNRAS*, 356, 1509  
 Curran S. J., Reeves S. N., Allison J. R., Sadler E. M., 2016b, *MNRAS*, 459, 4136  
 Curran S. J., Whiting M. T., 2010, *ApJ*, 712, 303  
 Curran S. J., Whiting M. T., 2012, *ApJ*, 759, 117  
 Curran S. J., Whiting M. T., Allison J. R., Tanna A., Sadler E. M., Athreya R., 2017b, *MNRAS*, 467, 4514  
 Curran S. J. et al., 2011, *MNRAS*, 416, 2143  
 Curran S. J. et al., 2011a, *MNRAS*, 413, 1165  
 Curran S. J., Whiting M. T., Murphy M. T., Webb J. K., Longmore S. N., Pihlström Y. M., Athreya R., Blake C., 2006, *MNRAS*, 371, 431  
 Curran S. J., Whiting M. T., Sadler E. M., Bignell C., 2013b, *MNRAS*, 428, 2053  
 Curran S. J., Whiting M. T., Tanna A., Sadler E. M., Pracy M. B., Athreya R., 2013c, *MNRAS*, 429, 3402  
 Curran S. J., Whiting M. T., Webb J. K., Athreya R., 2011b, *MNRAS*, 414, L26  
 Curran S. J., Whiting M. T., Wiklind T., Webb J. K., Murphy M. T., Purcell C. R., 2008, *MNRAS*, 391, 765  
 de Breuck C., van Breugel W., Stanford S. A., Röttgering H., Miley G., Stern D., 2002, *AJ*, 123, 637  
 de Vries W. H., Barthel P. D., O'Dea C. P., 1997, *A&A*, 321, 105  
 de Waard G. J., Strom R. G., Miley G. K., 1985, *A&A*, 145, 479  
 Emonts B. H. C. et al., 2010, *MNRAS*, 406, 987  
 Fanti C., 2000, in *EVN Symposium 2000, Proceedings of the 5th European VLBI Network Symposium*, Conway J. E., Polatidis A. G., Booth R. S., Pihlström Y. M., eds., Onsala Space Observatory, Chalmers Technical University, Göteborg, Sweden, p. 73  
 Fanti R., Fanti C., Schilizzi R. T., Spencer R. E., Nan Rendong, Parma P., van Breugel W. J. M., Venturi T., 1990, *A&A*, 231, 333  
 Feigelson E. D., Nelson P. I., 1985, *ApJ*, 293, 192  
 Field G. B., 1959, *ApJ*, 129, 536  
 Geréb K., Maccagni F. M., Morganti R., Oosterloo T. A., 2015, *A&A*, 575, 44  
 Grasha K., Darling J., 2011, in *American Astronomical Society Meeting Abstracts*, Vol. 43, p. 345.02  
 Grasha K., Darling J. K., Bolatto, A. D. Leroy A., Stocke J., 2018, *ApJ*, submitted  
 Gupta N., Salter C. J., Saikia D. J., Ghosh T., Jeyakumar S., 2006, *MNRAS*, 373, 972  
 Ishwara-Chandra C. H., Dwarakanath K. S., Anantharamaiah K. R., 2003, *JA&A*, 24, 37  
 Isobe T., Feigelson E., Nelson P., 1986, *ApJ*, 306, 490  
 Jalan P., Chand H., Srianand R., 2018, *ApJ*, submitted (arXiv:1809.04614)  
 Jones K. M., Ghosh T., Salter C. J., 2018, *AJ*, accepted (arXiv:1804.09225)  
 Kanekar N., Prochaska J. X., Ellison S. L., Chengalur J. N., 2009, *MNRAS*, 396, 385  
 Lavalley M. P., Isobe T., Feigelson E. D., 1992, in *BAAS*, Vol. 24, pp. 839–840  
 Ma C. et al., 2009, *IERS Technical Note*, 35, 1  
 Mirabel I. F., 1989, *ApJ*, 340, L13  
 Moore C. B., Carilli C. L., Menten K. M., 1999, *ApJ*, 510, L87  
 Morganti R., Oosterloo T. A., Tadhunter C. N., van Moorsel G., Killeen N., Wills K. A., 2001, *MNRAS*, 323, 331  
 Morganti R., Sadler E. M., Curran S., 2015, *Advancing Astrophysics with the Square Kilometre Array (AASKA14)*, 134  
 O'Dea C. P., 1998, *PASP*, 110, 493  
 Orienti M., Morganti R., Dallacasa D., 2006, *A&A*, 457, 531

- Peck A. B., Taylor G. B., Conway J. E., 1999, *ApJ*, 521, 103
- Peck A. B., Taylor G. B., Fassnacht C. D., Readhead A. C. S., Vermeulen R. C., 2000, *ApJ*, 534, 104
- Purcell E. M., Field G. B., 1956, *ApJ*, 124, 542
- Röttgering H., de Bruyn G., Pentericci L., Miley G., 1999, in *The Most Distant Radio Galaxies*, Röttgering H. J. A., Best P. N., Lehnert M. D., eds., p. 113
- Salter C. J., Saikia D. J., Minchin R., Ghosh T., Chandola Y., 2010, *ApJ*, 715, L117
- Schlegel D. J., Finkbeiner D. P., Davis M., 1998, *ApJ*, 500, 525
- Skrutskie M. F. et al., 2006, *AJ*, 131, 1163
- Srianand R., Gupta N., Momjian E., Vivek M., 2015, *MNRAS*, 451, 917
- Titov O., Malkin Z., 2009, *A&A*, 506, 1477
- Titov O., Stanford L. M., Johnston H. M., Pursimo T., Hunstead R. W., Jauncey D. L., Maslennikov K., Boldycheva A., 2013, *AJ*, 146, 10
- Uson J. M., Bagri D. S., Cornwell T. J., 1991, *PhRvL*, 67, 3328
- van Gorkom J. H., Knapp G. R., Ekers R. D., Ekers D. D., Laing R. A., Polk K. S., 1989, *AJ*, 97, 708
- Vermeulen R. C. et al., 2003, *A&A*, 404, 861
- Webster R. L., Francis P. J., Peterson B. A., Drinkwater M. J., Masci F. J., 1995, *Nat*, 375, 469
- Weymann R. J., Carswell R. F., Smith M. G., 1981, *ARA&A*, 19, 41
- Wild V. et al., 2008, *MNRAS*, 388, 227
- Wright E. L. et al., 2010, *AJ*, 140, 1868
- Yan T., Stocke J. T., Darling J., Hearty F., 2012, *AJ*, 144, 124
- Yan T., Stocke J. T., Darling J., Momjian E., Sharma S., Kanekar N., 2016, *AJ*, 151, 74